Optical Characteristics and Fault Diagnosis of Partial Discharge in C4F7N/CO2 Gas mixture and SF6 Based on Novel Multispectral Microarray Detection

Zang, Yiming; Qian, Yong; Zhou, Xiaoli; Niasar, Mohamad Ghaffarian; Sheng, Gehao; Jiang, Xiuchen

DOI
10.1109/TDEI.2022.3168332

Publication date
2022

Document Version
Accepted author manuscript

Published in
IEEE Transactions on Dielectrics and Electrical Insulation

Optical Characteristics and Fault Diagnosis of Partial Discharge in C_4F_7N/CO_2 Gas mixture and SF_6 Based on Novel Multispectral Microarray Detection

Yiming Zang, Yong Qian, Xiaoli Zhou, Mohamad Ghaffarian Niasar, Gehao Sheng, *Member*, *IEEE*, Xiuchen Jiang

***Abstract*—Optical partial discharge (PD) detection is an efficient means of diagnosing the insulation status of power equipment. C_4F_7N/CO_2 gas mixture is a very potential environmentally friendly SF_6 substitute gas, and its PD optical characteristics need to be studied to guide the PD diagnosis of novel C_4F_7N/CO_2 equipment. Therefore, this paper proposes a multispectral microarray detection technology, which can achieve high-sensitivity detection and PD diagnosis by simultaneously collecting the spectral characteristics of multiple bands. By setting up an experimental platform, the PD experiments of 4 typical defects in C_4F_7N/CO_2 gas mixture with 5 different proportions and pure SF_6 are carried out. Based on the analysis of PD multispectral features, the correlation between different gases and the difference between different defects are obtained. Finally, combining multispectral detection with t-distributed stochastic neighbor embedding (T-SNE) feature extraction algorithm, a PD diagnosis method that can adapt to both C_4F_7N/CO_2 gas mixture and SF_6 is proposed, which provides a reference for PD detection of novel C_4F_7N/CO_2 equipment application.**

***Index Terms*—C_4F_7N/CO_2 gas mixture, partial discharge, multispectral microarray detection, optical characteristic.**

I. Introduction

With the development of power grid technology, the application of gas insulated substations and equipment has become more extensive and important. At present, although SF_6 is used as the insulating gas in most of the gas insulation equipment, its serious greenhouse effect restricts its application, according to Kyoto Protocol list [1]. Research on the use of more environmentally friendly insulating gases has become crucial.

Fluoronitriles NOVEC™ 4710 (C_4F_7N) is a great potential alternative insulating gas to SF_6, which has excellent insulation performance and 10 times lower Global Warming Potential (GWP) value than that of SF_6 [2]. In application, C_4F_7N needs to be mixed with buffer gases such as CO_2, N_2 and dry air to reduce its higher liquefaction temperature. Existing studies have proven that C_4F_7N/CO_2 gas mixture is a more feasible insulation solution with better insulation and chemical properties. This gases mixture has been used in actual equipment which are currently in operation [3].

During the operation, partial discharge (PD) can occur due to manufacturing defects or inevitable deterioration of the insulation system over time. PDs may lead to unexpected equipment failure that can seriously threaten the safety and stability of the power grid [4]. Therefore, the detection of PD is a key means for evaluating the insulation status and early warning of equipment faults. At present, though online PD detection methods based on electromagnetic signals and ultrasonic signals are used [5, 6], they suffer from severe noise interference and signal attenuation in practical applications, which reduces the detection performance. The detection of PD optical signals can effectively avoid electromagnetic and vibration interference, and is a highly sensitive detection method with great application value [7].

However, the current research on C_4F_7N/CO_2 gas mixture equipment is mostly about its electrical insulation performance, decomposition characteristics and physical state [8-10]. There are very few studies on PD detection in C_4F_7N/CO_2 gas mixture, especially optical detection [11]. Moreover, most of the current optical detection is basically for SF_6 [12, 13]. The photons of PD are produced by multiple processes such as excitation, ionization, and recombination. Different gas molecules will produce photons of different wavebands, frequencies and scales, which will affect the characteristic distribution and diagnostic effects of optical detection [14]. Therefore, studying the difference between the optical characteristics of PD in C_4F_7N/CO_2 gas mixture and SF_6 is of great significance for the online PD detection of novel environmentally friendly gas-insulated equipment.

At present, the optical detection methods of PD mainly use intensified charge-coupled device (ICCD), photomultiplier tube (PMT) and silicon photomultiplier (SiPM) [15]. The ICCD and PMT are not conducive to practical application due to their complex, large and costly detection systems. SiPM is an optical sensor with high integration, high sensitivity and easy installation, which is very suitable for PD optical detection of gas insulated equipment. Nevertheless, the current method using SiPM can only detect a wide range of PD spectrum regions such as ultraviolet, visible and infrared [16]. The spectral resolution of the existing method is low, so that it is

This work was supported in part by the National Natural Science Foundation of China under Grant No. 62075045.

Yiming Zang, Yong Qian (*corresponding author*), Gehao Sheng and Xiuchen Jiang are with the Department of Electrical Engineering, Shanghai Jiao Tong University, Shanghai 200240, China (e-mail: zangyiming@sjtu.edu.cn; qian_yong@sjtu.edu.cn; shenghe@sjtu.edu.cn; xcjiang@sjtu.edu.cn).

Xiaoli Zhou is with the Department of Light Sources and Illuminating Engineering, School of Information Science and Technology, Fudan University, Shanghai 200433, China (e-mail: zhouxl@fudan.edu.cn).

Mohamad Ghaffarian Niasar is with the Electrical Sustainable Energy Department, Delft University of Technology, Mekelweg 4, 2628 CD, Delft, Netherlands (e-mail: M.GhaffarianNiasar@tudelft.nl).

difficult to detect the detailed information of the PD spectral characteristics.

In this paper, a PD optical detection method for gas-insulated equipment using the novel multispectral microarray detection is proposed. This method improves the spectral resolution of PD detection, which can better characterize the distribution and associated information of the PD spectral features in the C_4F_7N/CO_2 gas mixture and SF_6. Based on this high-resolution optical detection, pure SF_6 and gas mixture with 4%~12% C_4F_7N (96%~88% CO_2) were used to conduct PD experiments under 4 typical PD defects. Comparison and correlation between the PD multispectral characteristics in different insulating gases are discussed. At the same time, the spectral feature distribution and pulse repetition rate under different PD defects are studies. Finally, according to the differences in the time-domain characteristics of the PD multi-spectrum, a visual clustering diagnosis method for PD defects using t-distributed stochastic neighbor embedding (T-SNE) is proposed, which effectively solves the current challenges of PD defect diagnosis that require additional phase synchronization, and improves the compatibility of traditional optical detection methods in C_4F_7N/CO_2 gas mixture equipment.

II. Principle and Application of Multispectral Microarray Detection

A. Decomposition processes and principles of gas discharge

In the AC PD experiment, the AC power source can be regarded as an energy injection source. In this process, it can not only cause the local temperature of the gas to rise, but also produce high-energy electrons. The local temperature increase will cause the thermal degradation of the gas. The electron impact process will cause the ionization, dissociation and recombination of gas molecules. The main reactions in C_4F_7N/CO_2 gas mixture and SF_6 are shown below.

$$C_4F_7N \rightarrow (CF_3)_2CF+CN \quad (1)$$

$$(CF_3)_2CF \rightarrow (CF_3)_2C+F \quad (2)$$

$$CF_3CFCN \rightarrow CN+CF_3CF \quad (3)$$

$$CF_3CF \rightarrow C\text{-}CF_3+F \quad (4)$$

$$CF_2 \rightarrow CF+F \quad (5)$$

$$CO_2 \rightarrow CO+O \quad (6)$$

$$CO_2+O \rightarrow CO+O_2 \quad (7)$$

$$CO+O_2 \rightarrow CO_2+O \quad (8)$$

$$SF_6 \rightarrow SF_x+(6-x)F,\ x<5 \quad (9)$$

$$SF_x \rightarrow SF_{x-1}+F \quad (10)$$

$$SF_x^- + SF_6 \rightarrow F^- + SF_x + SF_5 \quad (11)$$

where (1) to (8) are some of the main reactions in the C_4F_7N/CO_2 gas mixture. Equation (9) to (11) are some of the main reactions in SF_6 [14, 17, 18].

At the same time, these different reactions will be accompanied by transitions of different electronic energy levels. When electrons transition from a high energy level to a low energy level, different emission spectra will be produced. The principle is as follows:

$$v = \frac{E_2 - E_1}{h} \quad (12)$$

$$\lambda = \frac{c}{v} \quad (13)$$

where v is the photon frequency, E_1 and E_2 is respectively the energy of low energy level and high energy level, h is Planck's constant, c is light speed constant.

Based on this principle, there must be differences in the PD spectral characteristics of C_4F_7N/CO_2 gas mixtures with different concentrations and SF_6, which will have a certain impact on optical PD detection. Therefore, multispectral analysis of C_4F_7N/CO_2 gas mixtures has important theoretical and practical significance.

B. Multispectral microarray detection

SiPM is a solid-state highly sensitive device based on single photon avalanche diodes (SPAD). The density of SPAD can be as high as 10000 per square millimeter. Each SPAD in SiPM operates in Geiger mode and is coupled with other SPADs through metal or polysilicon quenched resistors. All micro-units in SiPM are read in parallel, which makes it possible to generate optical signals in a dynamic range from a single photon to 1000 photons in an area of one square millimeter. In additional, its power supply voltage is 15 to 75 times lower than traditional PMT, which is conducive to the online operation of the sensor [19]. Compared with traditional ICCD spectrometer detection, the small-volume, highly integrated array layout improves the installability and scalability of the sensor, which is very conducive to multispectral PD detection of gas-insulated equipment.

In this paper, a novel type of multispectral microarray PD detection method is proposed based on the SiPM model ARRAYJ-30035-16P-PCB. This method takes advantage of the parallel collection of the SiPM detection unit, and installs a multispectral grid on the 4x4 sensor detection array. In Fig. 1, the different colors in the multispectral grid represents different kind of filters. Meanwhile, we design the corresponding collection circuit and analysis algorithm to realize the detection of the PD optical characteristics in different gases. Furthermore, a simulation of the PD light radiation distribution is carried out in Tracepro software, and it is verified that the received light intensity on the 16 grids is uniformly distributed due to the small photosensitive area of the sensor itself, which ensures the consistency of the detection, as shown in Fig. 1. The simulation model adopts the setting in Reference [20].

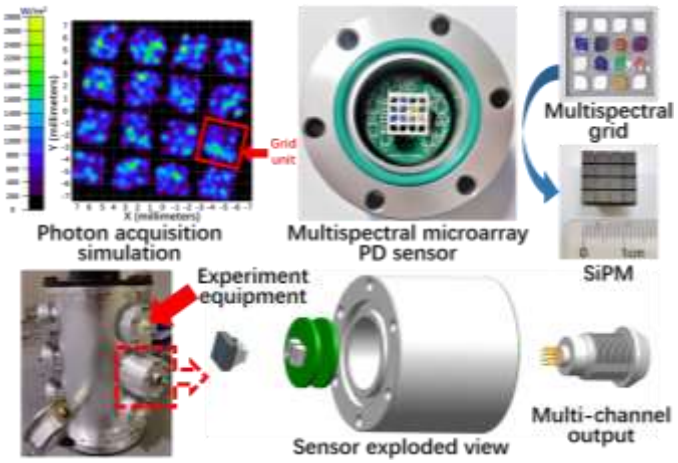

Fig. 1. Multispectral microarray sensor components and optical signal acquisition simulation.

Considering the detection range of the PD spectra, equipment cost and feature validity, six filters were selected for the experiments in this paper. Therefore, this paper selects 6 grid units to install different filters to detect 6 characteristic spectra in the full spectrum range. The remaining full band grid units are used as comparison and spare expansion units to improve the reliability and flexibility of the sensor. The transmittance range of the 6 spectral band (SB) is: SB1 (260~380 nm>90%), SB2 (400~445 nm>85%), SB3 (460~500 nm>90%), SB4 (510~545 nm>83%), SB5 (582~593 nm>85%), SB6 (630~1100 nm>90%). Because the photon detection efficiency (PDE) of SiPM is related to the spectral wavelength, the PDE of SiPM is shown in Fig. 2. The overvoltage in Fig. 2 represents two working states of the sensor.

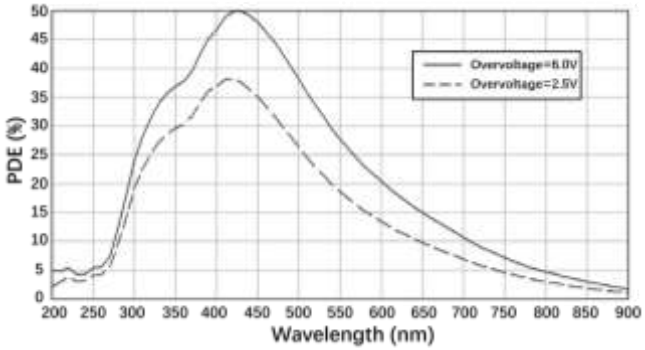

Fig. 2. PDE of SiPM (This paper uses 2.5V overvoltage).

C. PD experiment setup

The PD experiment setup is shown in Fig. 3. The high-voltage source is a corona-free AC source. The Haefely DDX 9121b PD detection instrument is used to detect the PD initial voltage (PDIV). The applied voltage of the PD test is 1.1PDIV. Because different defects have different PD voltages, the same value of voltage cannot be applied to all defects. Therefore, in order to improve the rationality of the experiment, we use the PDIV of each defect as the measure of the applied voltage, which makes each defect under the same voltage condition relative to itself. However, the PD of the defect may be unstable when the voltage is PDIV, and the breakdown may be easily caused when the voltage is too high than PDIV. Therefore, in order to obtain reliable experimental data more effectively, 1.1PDIV for each defect is chosen as the applied voltage for PD. Dynamic gas distribution instrument (GC400-2) is used to prepare gas mixtures with C_4F_7N/CO_2 ratios of 4%/96%, 6%/94%, 8%/92%, 10%/90%, and 12%/88%, to conduct the experiments under 0.2 MPa, and compare with pure SF_6. The selection of air pressure in this paper is based on the safety of the experimental equipment and practical applications. Although the propagation of the optical signal can be affected by the air pressure, the diagnosis method proposed in this paper is based on the relative values between different multispectral features rather than the absolute spectral intensity, so that the effect of air pressure on the detection method in this paper can be ignored. Therefore, an air pressure of 0.2 MPa is used in this paper within the range that the experimental tank can withstand the air pressure. PD tests for 4 types of defects were carried out for each kind of gas, including the needle defect, suspension defect, particle defect and creeping defect. A multi-channel acquisition card (HIOKI-MR6000) is used to synchronously acquire the output of the sensor. We collect 1000 ms PD data under each experiment condition.

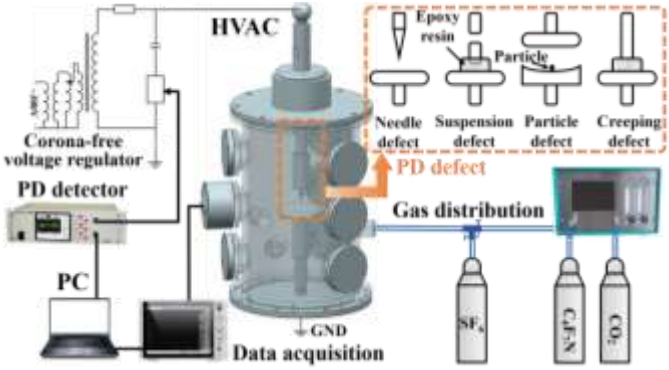

Fig. 3. Experiment setup of PD multispectral microarray detection.

III. Correlation of PD Spectral Features in Different Gases

The number of PD radiation photons can change with the severity of the discharge, but the relative proportions of different spectra are related to a certain degree. Therefore, this paper firstly calculates the sum of the light intensity detected by all SB in each PD pulse, and then calculates the percentage P_{in} (i=1~6, n is the number of PD pulse) of the light intensity detected by each SB to the total, which is regarded as the spectral feature of the SB. Finally, for all the detected PD pulses, their average values of each SB are calculated.

This paper introduces the Kendall correlation coefficient τ to quantitatively describe the correlation between the different spectral features of each SB. Let (x_1, y_1), …, (x_n, y_n) be a set of the joint random variables X and Y [21]. The Kendall correlation coefficient τ is defines as:

$$\tau = \frac{2}{n(n-1)} \sum_{i<j} \operatorname{sgn}(x_i - x_j) \operatorname{sgn}(y_i - y_j) \quad (14)$$

The coefficient is in the range -1< τ <1. When the Kendall correlation coefficient is 0, the two variables X and Y have no relationship. When the two variables are positively correlated, the coefficient τ is between 0~1. When two variables are negatively correlated, the coefficient is τ between -1~0. The greater the absolute value of the coefficient τ, the stronger the correlation.

The data for each kind of gas in Fig. 4 includes all 4 defect types, which can show the intrinsic relationship between different spectral features without considering the defect type. It can be seen from Fig. 4 that the average correlation of all features in each gas condition have similar correlation in general, but some of the features have relatively strong correlations.

In the gas mixture, SB1/SB3, SB1/SB4, SB1/SB5 and SB2/SB5 have a relatively strong negative correlation between the four pairs of spectral features. Among them, the negative correlation remains stable within a certain range. In SF_6, the negative correlations of SB1/SB2, SB1/SB3 and SB1/SB4 on the spectral features are relatively strong, and are significantly higher than that of C_4F_7N/CO_2 gas mixtures. In the C_4F_7N/CO_2 gas mixture and SF_6, the positive correlations between SB3/SB4 are both strong, and the correlation coefficients are similar. Among all the relationships, the correlation between SB2/SB3, SB2/SB4 and SB5/SB6 has the opposite correlation between C_4F_7N/CO_2 gas mixture and SF_6.

This shows that there is a certain correlation between some spectral features, which will cause information redundancy between the features. This phenomenon is caused by the before and after effects of the reaction of the discharge particles, as shown in Equation (1) to (11). There are also some spectral characteristics that are relatively stable, and remain basically independent of each other under different gas conditions. Therefore, in order to make better use of the collected multi-spectral data, independent and informative spectral characteristics are necessary to be extracted to describe the PD information.

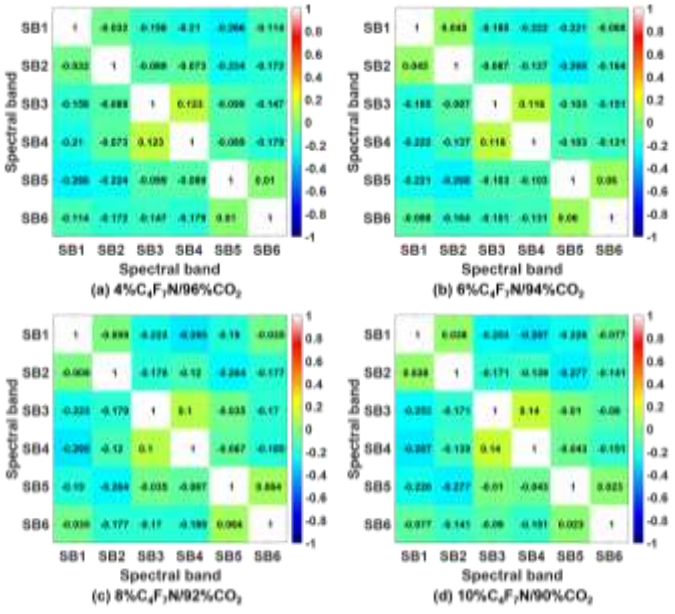

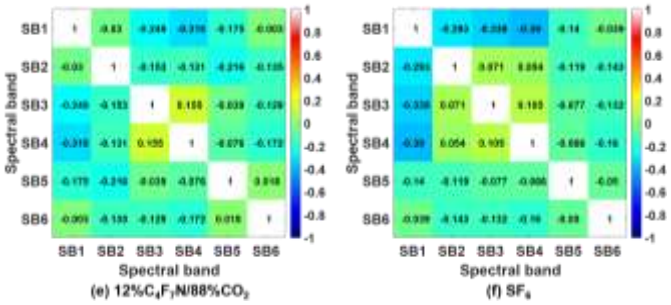

Fig. 4. Kendall correlation coefficients between PD multispectral features in different gases.

IV. Differences in Multispectral Features Between PD Defects

A. Multispectral intensity distribution

In order to better guide the optical PD detection of the C_4F_7N/CO_2 gas mixture insulation equipment, this paper compares the multispectral intensity distribution of PD defects in C_4F_7N/CO_2 and SF_6. Through experiments, it is found that the distribution of C_4F_7N/CO_2 gas mixtures of different concentrations is not much different, so the 4% C_4F_7N/96% CO_2 concentration that has been put into use in field equipment is selected for comparison with SF_6 [10].

In each experimental condition, we analyze all the P_{in} values to obtain a box distribution chart, which can describe the PD multispectral intensity distribution in two insulating gases under 4 kinds of defects. The box distribution chart in Fig. 5 shows the median, the lower and upper quartiles, and the minimum and maximum values that are not outliers.

It can be seen from Fig. 5 that the intensity distribution trends of the same defect in different gases are roughly similar, with only slight differences. However, the multispectral intensity distribution of the same gas under different defects is very different. Among them, the intensity ratio distribution of creeping defect is relatively wide, and the feature concentration is low. This shows that the multispectral distribution of different defects in the C_4F_7N/CO_2 gas mixture and SF_6 is more dominated by the types of PD defects, while the difference in gas types will have a relatively small effect.

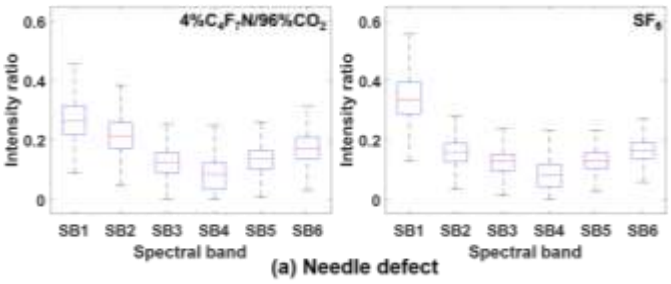

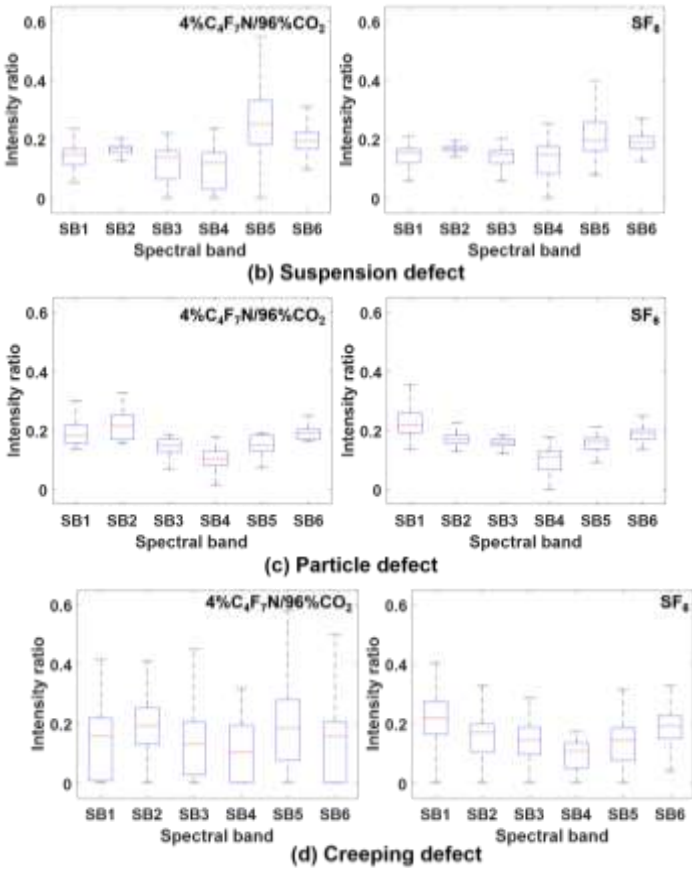

Fig. 5. Multispectral feature distribution of different types of defects in 4% C_4F_7N/96% CO_2 gas mixture and SF_6.

B. Multispectral difference feature distribution

According to the three Section above, there is some correlations between the multispectral features, so it has certain limitations to describe the multispectral features of different defects in different gases only by the intensity distribution of each SB. Therefore, in order to characterize the law of PD multispectral features in more detail, this paper introduces the concept of multispectral difference feature (MDF), which is defined as the absolute value of each SB feature subtracted from each other (15 in total). Take the average of all PD data in the 15 MDFs to obtain 15 average multispectral difference features (AMDF) as follows:

$$F_m = mean(\left|P_{in} - P_{jn}\right|),\ \begin{cases} i, j = 1,\ldots,6;\ i < j;\ i \neq j \\ n = 1,\ldots,N \\ m = 1,\ldots 15 \end{cases} \tag{15}$$

where F_m represents the m-th AMDF. P_{in} represents the spectral features of the n-th PD pulse collected by the i-th SB, and P_{jn} is the same. N represents the number of all PD pulses.

From the AMDF of the 4 defects in different gases in Fig. 6, it can be seen that the AMDF of different defects are significantly different overall, while the distribution trends of C_4F_7N/CO_2 gas mixture and SF_6 in the same defect are roughly similar. Because the PD of the needle defect and the suspension defect is relatively regular and stable, the distribution of various gases under these two defects is more similar. However, the randomness of the PD process of the particle defect and the creeping defect is relatively high, so the AMDF distribution of different gases has some fluctuations under these two defects.

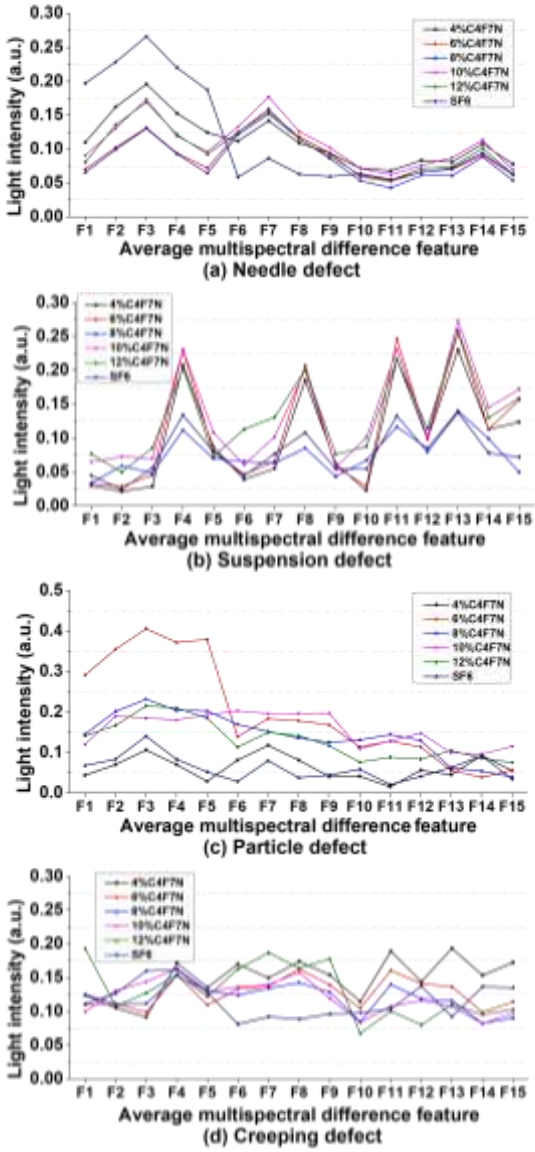

Fig. 6. Multispectral difference distribution.

In general, the C_4F_7N/CO_2 gas mixture and SF_6 have little difference in the multispectral intensity distribution and the multispectral difference distribution, basically can distinguish different types of PD, which means that the multispectral microarray technology proposed in this paper has the potential for PD diagnosis in both two gas insulating media. Therefore, in the next section, this paper proposes a corresponding optimization algorithm for PD fault diagnosis based on these two feature distributions.

V. PD Fault Clustering Diagnosis

A. PD pulse repetition rate

The multispectral microarray method adopted in this paper is based on the time-domain intensity signal, which reduces the problems of phase synchronization and data conversion

required for traditional detection. Therefore, after collecting the data, we can directly calculate the pulse repetition rate (PRR) of each PD defect in different gases, as shown in Table I. The percentage of C4 in Table I represents the proportion of C_4F_7N in the C_4F_7N/CO_2 gas mixture.

TABLE I
PD PULSE REPETITION RATE IN DIFFERENT GASES

Gas type	4%C4	6%C4	8%C4	10%C4	12%C4	Average PRR of C4 (pulses/ms)	SF_6
Needle defect	0.944	1.359	2.292	1.540	1.353	1.498	4.453
Suspension defect	0.121	0.106	0.100	0.099	0.095	0.104	0.116
Particle defect	0.045	0.045	0.053	0.056	0.064	0.053	0.112
Creeping defect	0.108	0.164	0.172	0.099	0.068	0.122	0.082

It can be seen from Table I that the PRR of C_4F_7N/CO_2 gas mixtures with different proportions in the same defect does not change too much, having some small fluctuations. Except for needle defects, there is a fluctuation at 8% C4 concentration. The average PRR of the needle defect, suspension defect and particle defect in the C_4F_7N/CO_2 gas mixture is lower than that in SF_6, and only the average PRR of the creeping defect in the C_4F_7N/CO_2 gas mixture is higher than that of SF_6.

By comparing the PRR between different defect types, the PRR of the needle defect in C_4F_7N/CO_2 gas mixture and SF_6 are at least 10 times higher than the other three defects in corresponding gases, which has a large order of magnitude difference.

B. PD multispectral clustering diagnosis based on T-SNE

From the analysis in above sections, it can be seen that the multispectral intensity feature and the difference feature have the problem of feature overlap and correlation, which is not conducive to effectively expressing the PD characteristics. Therefore, this paper proposes to use the T-SNE algorithm to extract effective information and reduce the dimensionality of multispectral features to better characterize the PD properties of different defects. In this paper above, since the needle defect has obvious characteristics in PRR, it is easier to distinguish from the other three types of defects in the time-domain multispectral signal. Considering the visualization, this section uses feature dimensionality reduction and visual clustering to diagnose the remaining three types of PD defects. In addition, it is noting that this method is also suitable for needle defects.

T-SNE is one of the few algorithms that can preserve the local and global structure of data in the process of feature extraction and dimensionality reduction. In addition, T-SNE is also more suitable for nonlinear data, which can better transform data through probability similarity [22]. T-SNE applies Stochastic Neighbor Embedding (SNE) to the data, and converts the high-dimensional Euclidean distance between the data points into a conditional probability of similarity. The similarity of data point x_j to data point x_i is represented by the conditional probability $p_{j|i}$, defined as follow:

$$p_{j|i} = \frac{\exp(\frac{-\|x_i - x_j\|^2}{2\sigma^2})}{\sum_{k\neq i}\exp(\frac{-\|x_i - x_k\|^2}{2\sigma^2})} \tag{16}$$

where σ represents the variance.

The probabilities in the original space are defined as follow:

$$p_{ij} = \frac{(p_{i|j} + p_{j|i})}{2n} \tag{17}$$

where n represents the amount of data in the data set.

In order to avoid the crowding problem [22], T-SNE applies the Student t-distribution with a single degree of freedom. Based on this distribution, the probability at low dimension q_{ij} is defined as follow:

$$q_{ij} = \frac{(1+\|y_i - y_j\|^2)^{-1}}{\sum_{k\neq l}(1+\|y_k - y_l\|^2)^{-1}} \tag{18}$$

Then, T-SNE optimizes the KL (Kullback-Leibler) divergences between the q_{ij} and $p_{j|i}$, the cost function is as follows:

$$C = \sum_i \sum_j p_{ij} \log \frac{p_{ij}}{q_{ij}} \tag{19}$$

Thus, T-SNE realizes the mapping of high-dimensional input data x_i to low-dimensional output data y_i by using gradient-based method.

Based on the T-SNE technology, we perform feature reduction processing on the PD multispectral data in C_4F_7N/CO_2 gas mixture and SF_6, which are divided into 4 feature conditions (FC) in total as follow, as shown in Table II:

TABLE II
FOUR DIFFERENT FEATURE PROCESSING METHODS

Feature condition	Feature processing method
FC1	6 original multispectral intensity features: *P*
FC2	15 multispectral difference features: *F*
FC3	*P* are reduced to 3 dimensional features by T-SNE
FC4	*F* are reduced to 3 dimensional features by T-SNE

In order to quantitatively evaluate the feature clustering performance under different FCs, this paper introduces the Silhouette index (SI) to measure it, which is defined as [23]:

$$S(i) = \frac{(b_i - a_i)}{\max(a_i, b_i)} \tag{20}$$

where a_i is the average distance from the i-th point to the other points in the same cluster as point i. b_i represents the minimum average distance from the i-th point to points in a different cluster, minimized over clusters. When there are a total of M points, the SI value in this condition can be expressed as:

$$\mathrm{SI} = \frac{\sum_{i=1}^{M} S(i)}{M} \tag{21}$$

The overall SI of the data set can be obtained by calculating the average SI of all points in different defects. The value of SI is between -1 and 1. The larger the value, the better the feature discrimination of the data under this characteristic condition, which means it has stronger clustering ability. The overall SI of the two gases under the four FCs is shown in Table III.

TABLE III
SILHOUETTE INDEX OF MULTISPECTRAL PD DATA UNDER DIFFERENT FEATURE CONDITIONS

Feature condition	FC1	FC2	FC3	FC4
4%C_4F_7N/CO_2	-0.291	-0.317	0.070	0.125
SF_6	-0.074	-0.107	0.072	0.113

It can be seen from Table III that under the conditions of FC1 and FC2, the SI of the C_4F_7N/CO_2 gas mixture is at least 20 times lower than that of SF_6, indicating that the direct multispectral feature describes the PD characteristics of C_4F_7N/CO_2 gas mixture weaker than that of SF_6. This may be due to the fact that there are more types of discharge molecules in the C_4F_7N/CO_2 gas mixture, which results in the overlap of spectral characteristics. If the PD data under FC1 and FC2 conditions are directly used for clustering diagnosis, the clustering performance of C_4F_7N/CO_2 gas mixture will be relatively poor. However, under the conditions of FC3 and FC4, the SI difference between the C_4F_7N/CO_2 gas mixture and SF_6 are very small, and both have increased. Because FC3 and FC4 are features that have been extracted by T-SNE, this shows that T-SNE improves the degree of feature aggregation between the same kind of defects, making defect clustering and diagnosis more effective.

Regarding the increase of SI from FC1/FC2 to FC3/FC4, it can be seen that the increase of C_4F_7N/CO_2 gas mixture is higher than that of SF_6, indicating that T-SNE has a more obvious advantage in C_4F_7N/CO_2 gas mixture. This advantage also better compensates for the weaker original feature information of the C_4F_7N/CO_2 gas mixture.

In addition, comparing FC1/FC3 and FC3/FC4, it can be obtained that the SI of the multispectral intensity feature is higher than the multispectral difference feature before dimensionality reduction, but that is lower than the multispectral difference feature after T-SNE. This shows that the FC4 has richer and more comprehensive PD information after the T-SNE, which is more suitable for PD diagnosis. Therefore, this paper uses the multispectral features under FC4 to perform the visual clustering analysis of PD, as shown in Fig. 7.

This article directly distinguishes the needle defect according to the PRR of the collected signal. Then, based on the visualized multispectral feature distribution under FC4, different remaining defect types can be clustered intuitively and effectively. Therefore, this method can directly use the collected multispectral time-domain data, avoiding the need to add a voltage synchronization device and phase information processing in the traditional clustering method. Importantly, the application of T-SNE makes the characteristic distribution of the C_4F_7N/CO_2 gas mixture more obvious, which is basically equivalent to that of SF_6. This is conducive to applying the PD diagnosis method of SF_6 equipment to new environmentally friendly gas-insulated equipment more compatible.

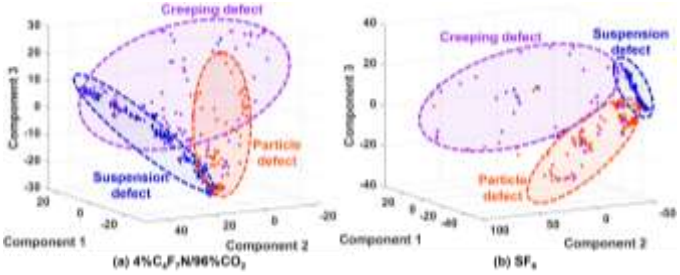

Fig. 7. Multispectral feature distribution of different defects under FC4.

VI. CONCLUSION

In this paper, a novel type of multispectral microarray sensor is designed to detect PD phenomena C_4F_7N/CO_2 gas mixture with different ratios and SF_6. By studying the similarities and differences between C_4F_7N/CO_2 gas mixture and SF_6 in the multispectral feature correlation, characteristic distribution and defect clustering diagnosis effect of PD, the new influence of C_4F_7N/CO_2 gas mixture on PD detection is revealed. The research results can help guide the future operation, and maintenance of new environmentally-friendly gas-insulated equipment. The specific conclusions are as follows:

(1) The novel multispectral microarray detection can realize the simultaneous acquisition of multi-channel spectral signals, which can directly and efficiently capture the PD optical information in more detail. In addition, the sensor not only takes into account high sensitivity, practicability and scalability, but also can intuitively diagnose PD defects avoiding additional phase synchronization process.

(2) In the C_4F_7N/CO_2 gas mixture and SF_6, there is a certain correlation between the multispectral features, and the strength of the correlation is related to the concentration and kind of the gas. For the multispectral feature distribution of different PD defects, the C_4F_7N/CO_2 gas mixture and SF_6 have almost similar distribution characteristics under the same type of defect.

(3) In the diagnosis of PD clustering, the distinguishability of the original multispectral features in the C_4F_7N/CO_2 gas mixture is lower than that of SF_6, which is not conducive to the PD diagnosis. In this paper, the feature clustering performance of C_4F_7N/CO_2 gas mixture and SF_6 has both been improved by T-SNE algorithm to achieve basic similarity. Moreover, the visual clustering analysis prove that this method helps to improve the compatibility of optical PD detection in traditional SF_6 equipment on C_4F_7N/CO_2 gas mixture equipment.

REFERENCES

[1] F. Ye *et al*, "AC Breakdown Strength and Its By-Products of Eco-Friendly Perfluoroisobutyronitrile/O2/N2 Gas Mixture at High Pressure for HV Equipment," IEEE Trans. Dielectr. Electr. Insul., vol. 28, no. 3, pp. 1020-1027, 2021.

[2] H. E. Nechmi *et al*, "Fluoronitriles/CO2 gas mixture as promising substitute

to SF6 for insulation in high voltage applications," IEEE Trans. Dielectr. Electr. Insul., vol. 23, no. 5, pp. 2587-2593, 2016.
[3] Y. Zheng *et al*. "Experimental and calculation study on insulation strength of C4F7N/CO2 at low temperature," IEEE Trans. Dielectr. Electr. Insul., vol. 27, no. 4, pp. 1102-1109, 2020.
[4] W. Fei *et al*, "Short-term Prediction of GIS Partial Discharge Based on ARMA Model," *IEEE Intern. Conf. on High Volt. Eng. and Appl. (ICHVE)*, 2020, pp. 1-4.
[5] D. Wang *et al*, "UHF PD measurement system with scanning and comparing method," IEEE Trans. Dielectr. Electr. Insul., vol. 25, no. 1, pp. 199-206, 2018.
[6] H. Karami *et al*, "An Acoustic Time Reversal Technique to Locate a Partial Discharge Source: Two-Dimensional Numerical Validation," IEEE Trans. Dielectr. Electr. Insul., vol. 27, no. 6, pp. 2203-2205, 2020.
[7] Y. Zang *et al*, "A Novel Optical Localization Method for Partial Discharge Source Using ANFIS Virtual Sensors and Simulation Fingerprint in GIL," IEEE Trans. Instrum. Meas., vol. 70, pp. 1-11, 2021.
[8] Y. Yang *et al*, "Review of the Decomposition Characteristics of Eco-friendly Insulation Gas," High Volt., vol. 6, no. 5, pp. 733-749, 2021.
[9] M. Ranković *et al*, "Temporary anions of the dielectric gas C3F7CN and their decay channels," J. Chem. Phys., vol. 152, no. 24, pp. 244304, 2020.
[10] Y. Tu *et al*, "Insulation characteristics of fluoronitriles/CO2 gas mixture under DC electric field," IEEE Trans. Dielectr. Electr. Insul., vol. 25, no. 4, pp. 1324-1331, 2018.
[11] C. Toigo *et al*, "Partial discharge behavior of protrusion on high voltage conductor in GIS/GIL under high voltage direct current: Comparison of SF6 and SF6 alternative gases," IEEE Trans. Dielectr. Electr. Insul., vol. 27, no. 1, pp. 140-147, 2020.
[12] S. Yoshida *et al*, "Light emission spectrum depending on propagation of partial discharge in SF6," *Conf. Rec. of IEEE Inter. Symp. on Electr. Insul. (ISEI)*, 2008, pp. 365-368.
[13] A. Lemzadmi *et al*, "Light emission from corona discharge in SF6 and SF6/N2 gas mixtures at high pressure," Eur. Phys. J.-Appl. Phys., vol. 33, no. 3, pp. 213-219, 2006.
[14] F. Y. Chu, "SF6 decomposition in gas-insulated equipment," IEEE Trans. Dielectr. Electr. Insul., vol. EI-12, no. 5, pp. 693-725, 1986.
[15] H. Zhou *et al*, "Optical sensing in condition monitoring of gas insulated apparatus: a review," High Volt., vol. 4, no. 4, pp. 259-270, 2019.
[16] M. Ren, J. Zhou and J. Miao, "Adopting Spectral Analysis in Partial Discharge Fault Diagnosis of GIS With a Micro Built-in Optical Sensor," IEEE Trans. Power Deliv., vol. 36, no. 2, pp. 1237-1240, 2020.
[17] S. Dobrea *et al*, "Optical and mass spectrometry diagnosis of a CO2 microwave plasma discharge," Rom. Rep. Phys., vol. 66, no. 4, pp. 1147-1154, 2014.
[18] B. Zhang *et al*, "Decomposition characteristics of C4F7N/CO2 mixture under AC discharge breakdown," AIP Adv., vol. 9, no. 11, pp. 115212, 2019.
[19] F. Meddi *et al*, "A new fast silicon photomultiplier photometer," Publ. Astron. Soc. Pac., vol. 124, no. 915, pp. 448-453, 2012.
[20] Y. Zang *et al*, "Method of GIL partial discharge localization based on natural neighbour interpolation and ECOC - MLP - SVM using optical simulation technology," High Volt., vol. 6, no. 3, pp. 514-524, 2021.
[21] D. Valencia, R. E. Lillo and J. Romo, "A Kendall correlation coefficient between functional data," Adv. Data Anal. Classif., vol. 13, no. 4, pp. 1083-1103, 2019.
[22] B. M. Devassy and S. George, "Dimensionality reduction and visualisation of hyperspectral ink data using t-SNE," Forensic Sci.Int., vol. 311, pp. 110194, 2020.
[23] P. J. Rousseeuw, "Silhouettes: a graphical aid to the interpretation and validation of cluster analysis," J. Comput. Appl. Math., vol. 20, pp. 53-65, 1987.

Yiming Zang (S'19) was born in Shandong, China, in 1996. He received a B.E. degree in electrical engineering from Southwest Jiao Tong University, Chengdu, China, in 2018. He is currently working toward a Ph.D. degree in electrical engineering at Shanghai Jiao Tong University. His research interests include online monitoring and fault diagnosis for power equipment insulation.

Yong Qian was born in Hubei, China. He received B.E. and M. Eng. degrees from Dalian Maritime University, China, in 2000 and 2003, respectively, and a Ph.D. degree from Shanghai Jiao Tong University, China, in 2007. He joined Shanghai Jiao Tong University in 2007. He has been involved in the development of PD monitoring systems since 2003. His major research interests include PD detection, PD signal processing, PD pattern analysis and the development of online/offline PD detection and evaluation systems.

Xiaoli Zhou was born in Henan, China. She received an M.Eng. degree from Xi'an Jiao Tong University, China, in 2003 and a Ph.D. degree from Fudan University, China, in 2010. She has been involved in research and teaching at Fudan University since 2003. Her major research interests include optoelectronic systems and control technology, LED illumination applications (drivers, lenses and packaging) and LED evaluation methods and systems.

Mohamad Ghaffarian Niasar was born in Tehran, Iran in 1984. He received the M.Sc. degree from Sharif University of Technology, Tehran, Iran in 2008, and Ph.D. degree in Electrical Engineering from Royal Institute of Technology (KTH) in Stockholm, Sweden, 2015. He is currently an assistant professor at DC System, Energy Conversion & Storage group in Technical University of Delft, in Netherlands. His main research interests are aging of electrical insulation, HVDC (High Voltage Direct Current) insulation system, partial discharges, high frequency power transformers, power cables, and FEM (Finite Element Modeling) modeling.

Gehao Sheng (M'08) was born in Hunan, China, in 1974. He received B.E., M.S., and Ph.D. degrees in electric power system and automation engineering from Huazhong University of Science and Technology, Wuhan, China, in 1996, 1999, and 2003, respectively. He is currently a Professor with the Department of Electrical Engineering, Shanghai Jiao Tong University, Shanghai, China. His research interests include condition monitoring for power apparatus.

Xiuchen Jiang was born in Shandong, China, in 1965. He received a B.E. degree in electrical engineering from Shanghai Jiao Tong University, Shanghai, China, in 1987; an M.S. degree in high voltage and insulation technology from Tsinghua University, Beijing, China, in 1992; and a Ph.D. degree in electrical engineering from Shanghai Jiao Tong University in 2001. He is currently a Professor with the Department of Electrical Engineering, Shanghai Jiao Tong University. His research interests include online monitoring, condition-based maintenance, and automation for electrical equipment.